

# Compression Field Modeling of Confined Concrete: Constitutive Models

Esneyder Montoya<sup>1</sup>; Frank J. Vecchio, M.ASCE<sup>2</sup>; and Shamim A. Sheikh, M.ASCE<sup>3</sup>

**Abstract:** It has been widely recognized that the behavior of confined concrete depends upon the level of confinement. Brittleness or ductility is a function of the state of compressive stresses, unconfined concrete strength, volumetric expansion, and concrete softening. Constitutive models for strength enhancement, concrete dilatation, and a new stress-strain relationship for concrete in triaxial compression are proposed. The load-carrying capacity of confined concrete is predicted by utilizing an Ottosen-type surface with newly developed coefficients that account for a wide range of confinement levels (lateral pressures up to 100% of the unconfined concrete strength) and unconfined concrete strengths from 20 to 130 MPa. Concrete dilatation is modeled as a function of the lateral pressure ratio and concrete strength and can reach values beyond the limit of incompressibility. Experimental results are used to corroborate the new models at the material level, producing accurate agreement.

**DOI:** 10.1061/(ASCE)0899-1561(2006)18:4(510)

**CE Database subject headings:** Concrete; Constitutive models; Triaxial compression; Stress strain relations.

## Introduction

Triaxial compressive stresses delay expansion and damage propagation in concrete. As concrete stresses become larger, the internal structures of paste, aggregates, and pores change. Cracks develop through the aggregates, pores collapse, and the failure mode transforms from brittle to ductile (Sfer et al. 2002). It is also well known that confinement increases the strength and ductility of concrete. After peak strength, low-confined concrete exhibits softening and decreasing capacity, whereas high-confined concrete exhibits continuous hardening behavior with little or no softening until failure.

Concrete subassemblies, elements, and structures subjected to triaxial stresses can be found in many civil engineering applications. In prestressed beams, anchorage of strands at the ends creates disturbed zones (D zones) that require stirrups around prestressed cables to prevent the concrete from spalling off explosively. Anchor fasteners embedded in concrete and subjected to tension produce high axisymmetric triaxial compressive stresses in the concrete in the vicinity of the bolt head (Pivonka et al. 2000). Concrete in massive dams is subjected to triaxial compression due to its self-weight and to restraints at the dam's base and lateral supports. Finally, reinforced concrete columns are passively confined by either steel, fiber-reinforced polymer (FRP)

fabric, or a combination of both. The behavioral enhancement of FRP composites for structural retrofitting has long been investigated [e.g., Demers and Neale (1999)].

Several types of formulations have been used in the analysis of concrete columns confined by steel stirrups or spirals, from simple empirical models [e.g., Sheikh and Uzumeri (1980); Mander et al. (1988)] that utilize physical variables (stirrup and longitudinal reinforcement arrangements, section dimensions, and material properties) to finite-element analysis techniques [e.g., Sankarasubramanian and Rajasekaran (1996); Montoya et al. (2001); Sfer et al. (2002)] based on nonlinear elasticity, plasticity, fracture mechanics, or continuum damage mechanics.

The work of several researchers has contributed to calibrating the behavior of confined concrete and has added to the database of experimental results. Measured lateral and axial strains at ultimate on concrete specimens have shown ratios of lateral to axial strain greater than 1.0 (Candappa et al. 1999); ratios larger than 6.0 in some uniaxial compression tests had also been found (Lee et al. 1997). It had also been observed that concrete dilatation depends on the level of lateral pressure (Assa et al. 2001a).

Several computational models for confined concrete had been proposed. Some of the proposed failure and loading surfaces of plasticity-type models used Drucker-Prager models (Karabinis and Rousakis 2002; Pivonka et al. 2000), which did not reproduce accurately the volumetric strain behavior. Many of the models require a large number of parameters to be calibrated, and the parameters applied to certain types of analyses had to be redetermined for other loading paths (Ghazi et al. 2002). These parameters are generally based on experimental results for one type of concrete (e.g., normal strength concrete or high-strength concrete) and could only be applied according to their constraints. Analytical stress-strain curves obtained by Sankarasubramanian and Rajasekaran (1996) were stiffer than the experiments, some of the curves did not reach peak stress, and either the analytical model was not able to trace the postpeak behavior, or the postpeak behavior did not follow that of the test.

Models based on compatibility of deformations and simple formulations for concrete strength [e.g., Assa et al. (2001a,b)]

<sup>1</sup>Senior Structural Designer, CHM Structural Engineers, Miami, FL 33156. E-mail: esneyder@chm.cc

<sup>2</sup>Professor, Dept. of Civil Engineering, Univ. of Toronto, 35 St. George St. Office 213, Canada M5S 1A4.

<sup>3</sup>Professor, Dept. of Civil Engineering, Univ. of Toronto, 35 St. George St. Office 213, Canada M5S 1A4.

Note. Associate Editor: Kiang-Hwee Tan. Discussion open until January 1, 2007. Separate discussions must be submitted for individual papers. To extend the closing date by one month, a written request must be filed with the ASCE Managing Editor. The manuscript for this paper was submitted for review and possible publication on December 20, 2004; approved on May 20, 2005. This paper is part of the *Journal of Materials in Civil Engineering*, Vol. 18, No. 4, August 1, 2006. ©ASCE, ISSN 0899-1561/2006/4-510-517/\$25.00.

made several assumptions that rendered them useful to reproduce the general behavior of structural elements with certain types of cross sections (e.g., circular sections). However, they gave no insight on the distribution of confinement between ties or within the cross section of the column.

This paper describes a new and complete set of constitutive models developed to analyze confined concrete. The models include a stress-strain curve that accounts for 3D effects, concrete dilatation, strength enhancement, postpeak softening, or increased strain hardening. The concretes studied cover all types of commercially available concrete, from low strength (20 MPa) to very high strength (130 MPa), and a large range of confining pressures, from zero confinement up to a lateral pressure equal to 100% of the unconfined concrete strength.

Simple relationships between the type of concrete and the confinement level (ratio of lateral pressure to unconfined concrete strength) were established to develop coefficients to modify the parameters of a well-known failure surface whose original version does not cover the wide range of experimental data published, especially those of high concrete strengths and high confinement. Concrete dilatation depends upon the exerted lateral pressure and the type of concrete and was not bounded by the incompressible Poisson's ratio limit of 0.5. All the relationships are given in terms of stresses and strains, which make them suitable for incremental nonlinear elastic finite-element analysis and for a wide range of structural applications and types of confinement (e.g., constant lateral pressure and steel- and FRP-confined concrete).

## Research Significance

The difficulties in obtaining experimental results (e.g., strains) in concrete specimens, such as pullout tests of bolts, prestressed anchorages, and scaled models of concrete dams, just to mention some, have led to the formulation of material behavior models based on simpler tests (e.g., cylinder specimens) and the extrapolation of those models to analyze more complex subassemblies. Finite-element techniques provide useful insight on material behavior, and well-engineered models and numerical analyses contribute to the design of experimental tests and the determination of simple formulations for design purposes based on realistic material and structural behavior.

## Constitutive Models

Three basic constitutive models were developed to analyze concrete behavior when confined: expressions for concrete dilatation, the strength gain of concrete in a triaxial stress state, and a complete stress-strain curve for confined concrete.

## Concrete Dilatation

Experimental results of concrete cylinders subjected to triaxial compressive stresses, obtained from a testing program carried out by Imran and Pantazopoulou (1996), were used to formulate a simple model for concrete dilatation. The cylinders had a diameter of 54 mm and a height of 108 mm. The target unconfined concrete strengths  $f'_c$  were 65, 43, and 21 MPa, and the water/cement ratios utilized were 0.4, 0.55, and 0.75. The cylinders were subjected to seven target levels of confinement (i.e., ratio of

lateral pressure to unconfined concrete strength  $f_{cl}/f'_c$ )—0, 0.05, 0.10, 0.20, 0.40, 0.70, and 1.00—and four different load paths. From the 130 cylinders tested, only those cylinders subjected to constant lateral pressure and monotonic axial compression and tested under “dry” conditions were investigated. At the time of testing, the unconfined strengths were 73.4, 47.4, and 28.6 MPa, respectively. The experimental results were plotted in curves of lateral strain  $\varepsilon_{cl}$ –axial strain ratio ( $\varepsilon_c/\varepsilon_{cc}$ ) (axial and lateral strains positive,  $\varepsilon_c$  being the axial strain and  $\varepsilon_{cc}$  the strain at peak stress) and fitted to a parabola

$$\varepsilon_{cl} = \alpha \left( \frac{\varepsilon_c}{\varepsilon_{cc}} \right)^2 \quad (1)$$

where  $\alpha$  = fitting parameter. A linear correlation was found between  $\alpha$  and the lateral pressure ratio  $f_{cl}/f'_c$  for all the concrete strengths. The value of  $\alpha$  increases with an increase in the lateral pressure ratio or confinement level. The statistical correlation can be found elsewhere (Montoya 2003). The equation for lateral strain given above can be expressed in terms of the confinement ratio as

$$\varepsilon_{cl} = \left( 1.9 + 24.2 \frac{f_{cl}}{f'_c} \right) \left( \frac{\varepsilon_c}{\varepsilon_{cc}} \right)^2 \quad (2)$$

Considering the initial Poisson's ratio  $\nu_o$ , the secant Poisson's ratio  $\nu$  is proposed to be calculated as

$$\nu = \left( 1.9 + 24.2 \frac{f_{cl}}{f'_c} \right) \frac{\varepsilon_c}{\varepsilon_{cc}^2} + \nu_o \quad (3)$$

## Strength Enhancement

The parameters considered to affect the strength gain of triaxial compressed concrete are the level of confinement and the type of concrete. Experimental results of strength enhancement in columns subjected to monotonic axial compression and small concrete cylinders subjected to active lateral pressure and axial compression, observed in more than 280 specimens and described in Tables 1 and 2, have led to the definition of two simple categories of concrete types and confinement ratios, respectively, accounting for a reasonable spectrum of possible ranges of confined behavior of concrete.

From the data in Tables 1 and 2 the following conclusions may be drawn. About 96% of the total number of column specimens studied reached a level of confinement between 0 and 20%, that is,  $f_{cl}/f'_c \leq 0.20$  for concrete strengths from 20 to 130 MPa. It was also found that the confinement level tends to decrease with an increase in the unconfined concrete strength, which may be expected due to the reduced lateral dilatation of high-strength concrete (HSC). The average number of columns per concrete strength range was 24, with 86% of the total number of columns having unconfined strengths  $\leq 100$  MPa.

In the case of the concrete cylinders, about 63% of the cylinders were subjected to active pressure ratios  $\leq 20\%$ , 31% to pressure ratios between 20 and 100%, and the remaining 6% to pressure ratios over 100%. The average number of specimens per concrete strength range was 15, with 70% of the cylinders with  $f'_c \leq 100$  MPa. From the observed data, two levels of confinement are defined:

- *Low confinement*: when a concrete element is subjected to an average lateral pressure ratio  $\leq 0.20$  in a plane normal to the major principal compressive stress (i.e.,  $f_{c3}$ ); and

**Table 1.** Description of Sets of Columns per Researcher(s)

Researcher(s)	Tests	Section size (mm)	$f'_c$ (MPa)		$f_{ci}/f'_c$	
			Maximum	Minimum	Maximum	Minimum
Sheikh and Uzumeri (1980)	22	305·305				
		305·305	40.86	31.28	0.22	0.03
		305·305				
Toklucu (1992)	26	356	35.90	34.90	0.19	0.02
		254				
		203				
Montgomery (1996)	15	305	89.80	69.70	0.17	0.01
		254				
Pessiki et al. (2001)	13	610	58.60	52.10	0.21	0.04
		356				
Razvi and Saatcioglu (1999) (circular)	16	230	105.40	51.00	0.08	0.02
Razvi and Saatcioglu (1999) (square)	24	230·230	105.40	51.00	0.13	0.03
Nagashima (Razvi and Saatcioglu 1999)	24	205·205	100.40	51.30	0.11	0.04
Nagashima (Razvi and Saatcioglu 1999)	14	220·220	96.20	92.40	0.16	0.04
Li (Razvi and Saatcioglu 1999)	14	210	82.50	52.00	0.32	0.03

• *High confinement*: when a concrete element is subjected to an average lateral pressure ratio  $>0.20$  in a plane normal to the major principal compressive stress.

The unconfined concrete strengths are divided into two ranges:

- *Normal strength concrete (NSC)*: when a concrete element has an unconfined concrete strength  $f'_c=40$  MPa; and
- *High-strength concrete (HSC)*: when a concrete element has an unconfined concrete strength  $f'_c > 40$  MPa.

Four categories of confinement result from combining the given definitions:

- *LN*=low-confined normal strength concrete;
- *HN*=high-confined normal strength concrete;
- *LH*=low-confined high-strength concrete; and
- *HH*=high-confined high-strength concrete.

These categories were used to calibrate a four-parameter Ottosen-type criterion in the principal stresses space ( $f_{c1}, f_{c2}, f_{c3}$ ), which can be represented by the following set of equations (compression negative):

$$a \frac{J_2}{f_c'^2} + \lambda \frac{\sqrt{J_2}}{f_c'} + b \frac{I_1}{f_c'} - 1 = 0; \quad (f_c' > 0) \quad (4)$$

$$\lambda = k_1 + k_2 \cdot \cos 3\theta \quad (5)$$

where the parameters are  $a, b, k_1,$  and  $k_2,$  and the stress invariants  $I_1, J_2, J_3$  are calculated as functions of the principal concrete stresses

$$\cos 3\theta = \frac{3\sqrt{3}}{2} \frac{J_3}{J_2^{3/2}}; \quad J_2 = \frac{1}{2}(s_1^2 + s_2^2 + s_3^2)$$

$$J_3 = \frac{1}{3}(s_1^3 + s_2^3 + s_3^3); \quad I_1 = f_{c1} + f_{c2} + f_{c3}$$

$$s_i = f_{ci} - \frac{1}{3}I_1; \quad i = 1, 2, 3 \quad (6)$$

### Proposed Ottosen Parameters

Four tests are needed to find the parameters of the Ottosen-type criterion: the uniaxial compressive test, a triaxial test to define the compressive meridian, the uniaxial tensile test, and a biaxial test

**Table 2.** Description of Sets of Cylinders per Researcher(s)

Researcher(s)	Tests	$\phi \cdot h$ (mm)	$f'_c$ (MPa)		$f_{ci}/f'_c$	
			Maximum	Minimum	Maximum	Minimum
Hurlbut (Pivonka et al. 2000)	4		22.06	22.06	0.63	0.03
Gardner (1969)	3	75·150	27.59	27.59	0.94	0.31
Ansari and Li (1998)	14	100·200	103.00	42.00	0.93	0.18
Richart et al. (1928)	16 <sup>a</sup>	100·200	25.24	7.24	3.90	0.07
Attard and Setunge (1996)	38	100·200	132.00	60.00	0.25	0.02
Imran and Pantazopoulou (1996)	18	54·108	64.70	21.20	1.00	0.05
Xie et al. (1995)	26	55.5·110	119.00	60.20	0.50	0.01

Notes:  $\phi$ =diameter; and  $h$ =height.

<sup>a</sup>Average of four tests.

**Table 3.** Proposed Values for Parameter  $a$ 

$f_{ct}$	LN	HN	LH	HH
$0.65f'_c{}^{0.33}$	17.097	2.406	17.447	15.061
$0.33f'_c{}^{0.5}$	18.717	2.942	10.615	13.913
$0.60f'_c{}^{0.5}$	8.070	1.103	4.633	6.668
$0.10f'_c$	8.143	1.586	1.976	3.573

to define the tensile meridian. Three of the parameters,  $b$ ,  $k_1$ , and  $k_2$ , are resolved in terms of the parameter  $a$  using the following boundary conditions:

- Uniaxial compression test:  $f_{c1}=f_{c2}=0$ ;  $f_{c3}=-f'_c$ ;  $(0, 0, -f'_c)$ ;
- Uniaxial tensile test:  $f_{c1}=f_{ct}$ ;  $f_{c2}=f_{c3}=0$ ;  $(f_{ct}, 0, 0)$ ; and
- Biaxial test:  $f_{c1}=0$ ;  $f_{c2}=f_{c3}=-f_{bc}$ ;  $(0, -f_{bc}, -f_{bc})$ .

where  $f_{ct}$  and  $f_{bc}$  are the concrete uniaxial tensile and biaxial compressive strengths, respectively. By solving the  $4 \times 4$  system of equations, the parameters  $b$ ,  $k_1$ , and  $k_2$  are

$$b = \frac{1}{9}a \left[ \frac{f_{bc} - f_{ct}}{f'_c} \right] + \frac{1}{3} \left[ \frac{f'_c}{f_{ct}} - \frac{f'_c}{f_{bc}} \right] \quad (7)$$

$$k_1 = \frac{\sqrt{3}}{2} \left\{ 1 + \frac{f'_c}{f_{ct}} - \frac{1}{3}a \left[ 1 + \frac{f_{ct}}{f'_c} \right] \right\} \quad (8)$$

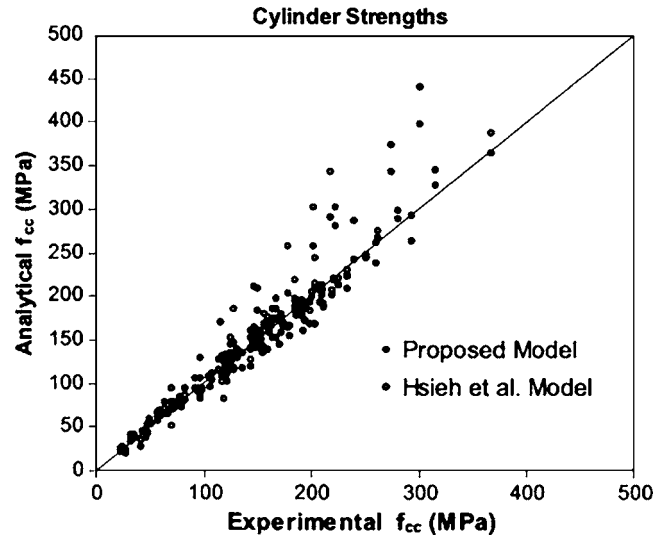
$$k_2 = \frac{\sqrt{3}}{2} \left\{ \frac{f'_c}{f_{ct}} - 1 - 2b - \frac{1}{3}a \left[ \frac{f_{ct}}{f'_c} - 1 \right] \right\} \quad (9)$$

The biaxial compressive strength  $f_{bc}$  is calculated from an approximation of the tests by Kupfer et al. (1969)

$$f_{bc} = 1.16f'_c \quad (10)$$

The Ottosen-type criterion [Eq. (4)] was fitted to the experimental results of the reinforced concrete columns and concrete cylinders presented in Tables 1 and 2. For columns, the average maximum concrete lateral pressure was used in the statistical fitting, and for cylinders it was considered that the lateral pressure was uniformly applied along the lateral surface of the cylinder. The proposed values for parameter  $a$  are given in Table 3 as a function of the tensile strength  $f_{ct}$ . Although the values for parameter  $a$  are discrete, the strength enhancement ratio (i.e., the ratio of strength  $f_{cc}$  to unconfined concrete strength  $f'_c$ ) showed a smooth transition among all the confinement categories except HN, which may be explained by the fact that the derived statistical value for  $a$  for confinement category HN was based on a limited number of tests (6% of total database).

This set of values for  $a$ , along with the corresponding values for  $b$ ,  $k_1$ , and  $k_2$ , is used to predict the concrete strength of the examined specimens. The criterion was compared with several failure surfaces proposed in the literature. For brevity, Fig. 1 only shows the comparison of the analytical and experimental strengths of concrete cylinders obtained with the proposed Ottosen-type criterion and those obtained with the Hsieh et al. criterion (Chen 1982). Table 4 shows the statistical comparisons of the proposed model and those by Hsieh et al., Drucker-Prager, Richart et al., and the original Ottosen model as described elsewhere (Montoya 2003), demonstrating the ability of the proposed criterion to better predict the concrete strength in a wide range of concrete types (from 20 to 130 MPa) and confinement ratios (from 0 to 100% of  $f'_c$ ).

**Fig. 1.** Comparison of cylinder strengths obtained with proposed model and Hsieh et al. model

### Strain at Peak Stress of Confined Concrete ( $\epsilon_{cc}$ )

The experimental data from the triaxial tests conducted by Ansari and Li (1998); Attard and Setunge (1996), and Imran and Pantazopoulou (1996) were used in a linear regression to propose a model to determine the strain at peak stress,  $\epsilon_{cc}$ . A linear relationship was found between the normalized strain at peak,  $\epsilon_{cc}/\epsilon_{co}$  ( $\epsilon_{co}$ =strain at peak unconfined stress  $f'_c$ ), and the confinement level  $f_{ct}/f'_c$

$$\frac{\epsilon_{cc}}{\epsilon_{co}} = 1.0 + k_{cc} \frac{f_{ct}}{f'_c} \quad (11)$$

where  $k_{cc}$ =factor that depends on the unconfined concrete strength  $f'_c$ . From the experimental results, it was evident that for a particular confinement level, the normalized strain at peak decreased with an increase in the concrete strength. The value of  $k_{cc}$  is given as

$$k_{cc} = 24.4 - 0.116f'_c \quad (12)$$

The experimental data set covered concrete strengths between 20 and 130 MPa and confinement levels ( $f_{ct}/f'_c$ ) from 0 to 1.0; a moderate correlation was found in Eq. (12) as the result of the scatter in the experimental strain data.

### Stress-Strain Curve for Confined Concrete

A formulation for the complete stress-strain curve for concrete subjected to triaxial compressive stresses is presented. The curve has two branches defined by different mathematical formulations. The complete confined concrete stress-strain curve is then used to corroborate a series of experimental results.

**Table 4.** Predicted Experimental Strength Ratios, Cylinders

	Hsieh et al.	Drucker-Prager	Richart et al.	Ottosen	Proposed model
Average	1.05	0.87	0.97	1.09	0.98
Standard deviation	0.151	0.191	0.156	0.147	0.120
COV (%)	14.45	21.86	16.10	13.44	12.80

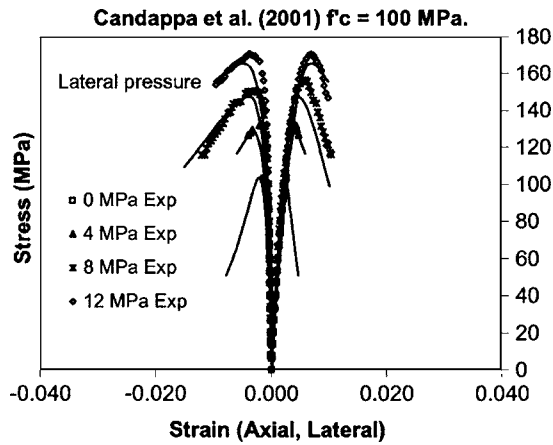


Fig. 2. Axial stress—(axial, lateral) strain curves, 100 MPa cylinders (adapted from Candappa et al. 2001)

### Prepeak Stress-Strain Curve

The stress-strain curve by Hoshikuma et al. (1996) was adopted to model the ascending branch of the compressive behavior of concrete. The stress  $f_c$  is related to the strain  $\epsilon_c$  using the following formula:

$$f_c = E_c \epsilon_c \left[ 1 + \frac{1}{n} \left( \frac{\epsilon_c}{\epsilon_{cc}} \right)^{n-1} \right] \quad (13)$$

$$n = \frac{E_c \cdot \epsilon_{cc}}{E_c \cdot \epsilon_{cc} - f_{cc}} \quad (14)$$

where  $E_c$  is the initial stiffness and  $\epsilon_{cc}$  is the strain at peak stress  $f_{cc}$ .

### Proposed Postpeak Stress-Strain Curve

The postpeak behavior is affected by the level of confinement; a curve based on the “witch of Agnesi” (Tume 1987) was developed to account for concrete softening after the peak stress. This curve depends on two parameters: the postpeak strain at 80% of the peak stress, and a shape factor  $K_d$ , which depends on the confining conditions of the concrete.

### Postpeak Strain at 80% of Peak Stress ( $\epsilon_{c80}$ )

The experimental data from the triaxial tests conducted by Ansari and Li (1998), Attard and Setunge (1996), Candappa et al. (2001), and Xie et al. (1995) were used to propose a model to determine

the strain  $\epsilon_{c80}$ , which was normalized with respect to the experimental strain at peak unconfined strength,  $\epsilon_{co}$ , that is,  $\epsilon_{c80}/\epsilon_{co}$ . When the postpeak range of the experimental curve did not decay sufficiently to reach the stress value corresponding to 80% of  $f_{cc}$ , the curve was approximated to a polynomial, and the strain value  $\epsilon_{c80}$  was calculated using the fitted curve.

A linear relationship between the normalized strain  $\epsilon_{c80}/\epsilon_{co}$ , and the confinement level  $f_{cl}/f'_c$ , is proposed to calculate the strain  $\epsilon_{c80}$  in the postpeak curve

$$\frac{\epsilon_{c80}}{\epsilon_{co}} = 1.5 + k \frac{f_{cl}}{f'_c} \quad (15)$$

where  $k$ =factor that depends on the unconfined concrete strength  $f'_c$ , as was the case with  $k_{cc}$ . The value for  $k$  is given by the equation (correlation factor of 0.83)

$$k = 89.5 - 0.60f'_c \quad (16)$$

### Shape Factor ( $k_d$ )

A shape factor,  $k_d$ , is proposed to force the postpeak curve to pass through the stress-strain point corresponding to 80% of the peak stress,  $0.80f_{cc}$ , that is,  $(\epsilon_{c80}, 0.80f_{cc})$ . The shape factor is an indicator of the steepness of the stress-strain curve beyond the peak strength. The “witch of Agnesi” is transformed in terms of stresses and strains in the following equation:

$$f_c = \frac{f_{cc}^3}{f_{cc}^2 + k_d(\epsilon_c - \epsilon_{cc})^2}, \quad \epsilon_c \geq \epsilon_{cc}, (\epsilon_c > 0) \quad (17)$$

when the strain  $\epsilon_c$  reaches the strain at peak,  $\epsilon_c = \epsilon_{cc}$ , the stress  $f_c$  becomes the peak strength  $f_{cc}$ . Replacing the point  $(\epsilon_{c80}, 0.80f_{cc})$  in the latter equation gives the following formulation for the shape factor  $k_d$ :

$$k_d = \frac{1}{4} \left( \frac{f_{cc}}{\epsilon_{c80} - \epsilon_{cc}} \right)^2 \quad (18)$$

where the values for the strains  $\epsilon_{c80}$  and  $\epsilon_{cc}$  are calculated using Eqs. (15) and (10), respectively, and the stress at peak  $f_{cc}$  is obtained from the proposed Ottosen-type criterion. Eq. (18) is mathematically modified to produce the final expression given below

$$f_c = \frac{f_{cc}}{A \left( \frac{\epsilon_c}{f_{cc}} \right)^2 - B \left( \frac{\epsilon_c}{f_{cc}} \right) + C + 1.0} \quad (19)$$

where

Table 5. Experimental and Analytical Curve Parameters of Candappa et al. Curves

Analytical								Experimental							
$f'_c$ (MPa)	$f_{cl}$ (MPa)	$\epsilon_{co}^c$ (10-3)	$\epsilon_{cc}$ (10-3)	$\epsilon_{c80}$ (10-3)	$k_d$ (10+8)	$f_{cc}$ (MPa)	$\epsilon_{cl}^b$ (10-3)	$\epsilon_{co}$ [10-3]	$\epsilon_{cc}$ [10-3]	$\epsilon_{c80}^a$ [10-3]	$f_{cc}$ (MPa)	$\epsilon_{cl}^b$ (10-3)	$\frac{f_{cc}(an)}{f_{cc}(exp)}$	$\frac{\epsilon_{cc}(an)}{\epsilon_{cc}(exp)}$	
100	0	2.38	2.38	3.57	18.91	103.5	-1.93	2.80	2.80	4.10	103.5	-1.14	1.00	0.85	
—	4	2.38	3.52	6.09	6.19	127.7	-2.90	2.80	3.91	8.50	132.4	-1.49	0.96	0.90	
—	8	2.38	4.67	8.61	3.51	147.7	-3.87	2.80	6.09	9.60	156.4	-2.65	0.94	0.77	
—	12	2.38	5.81	11.13	2.42	165.5	-4.83	2.80	7.11	11.30	170.7	-3.62	0.97	0.82	

<sup>a</sup>Estimated from experimental curve.

<sup>b</sup>Lateral strain at peak stress (negative).

<sup>c</sup>Calculated.

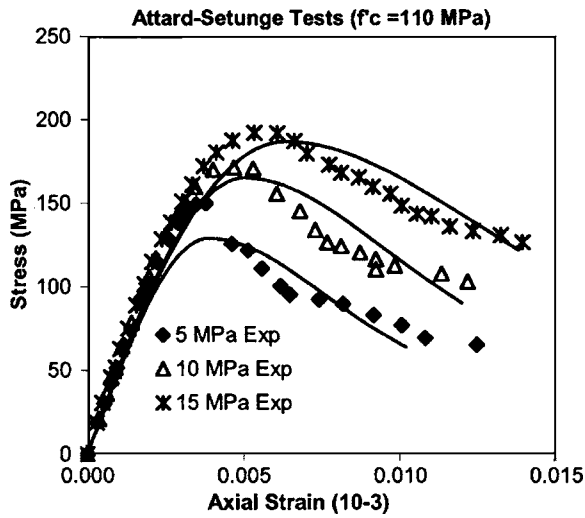


Fig. 3. Axial stress—axial strain curves, 100 MPa cylinders (data adapted from Attard and Setunge 1996)

$$A = k_d; \quad B = 2 \frac{A}{E_{sec}}; \quad C = \frac{A}{E_{sec}^2}; \quad E_{sec} = \frac{f_{cc}}{\epsilon_{cc}} \quad (20)$$

### Confined Behavior

This section examines the stress-strain curves obtained from experimental observations of concrete cylinders subjected to axial compression and either active lateral pressure or confinement with FRP composites. Experimental axial stress—axial strain curves and axial stress—lateral strain curves are compared with the analytical curves calculated using the proposed models. A brief description for each set of specimens is given along with the stress-strain plots. In all cases, the values for the parameter  $a$  corresponding to a tensile strength  $f_{ct} = 0.65f_c'^{0.33}$  were assumed in the analyses.

#### Candappa et al. (1999)

The axial stress—axial strain and axial stress—lateral strain curves for four of the concrete cylinders tested are shown here. The target concrete strength was 100 MPa, and the cylinders had a diameter of 98 mm and were 200 mm high. The cylinders were tested in monotonic axial compression and active lateral pressure applied using pressurized oil in a triaxial chamber. The cylinders were subjected to lateral pressures of 0, 4, 8, and 12 MPa, respectively. The peak strengths  $f_{cc}$ , strain at peak  $\epsilon_{cc}$ , and unconfined strain at peak  $\epsilon_{co}$ , were deduced from the experimental curves, as tabulated data were not given by Candappa et al. Fig. 2 shows the axial stress—(axial, lateral) strain curves for the specimens (axial

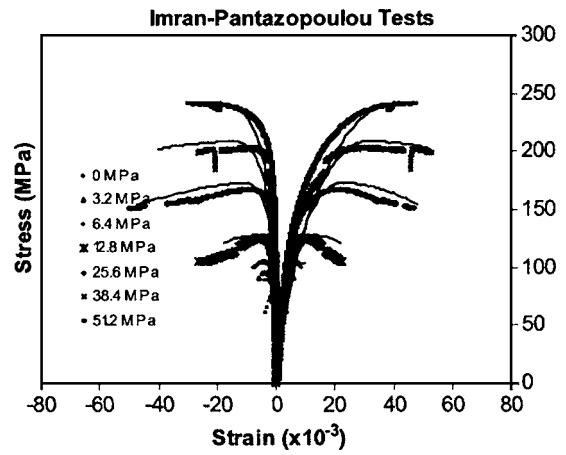


Fig. 4. Axial stress—(axial, lateral) strain curves, 73.4 MPa cylinders, Imran and Pantazopoulou tests

strain positive). The solid lines are the analytical curves, and the markers represent the experimental data. Table 5 shows the main parameters for each curve. Concrete strength and strain at peak stress are well captured by the proposed models for all cases. The lateral strain—axial stress curves obtained from the dilatation model follow the general trend of the concrete lateral expansion of the specimens.

#### Attard and Setunge (1996)

High-strength concrete cylinders with unconfined concrete strengths ranging from 60 to 130 MPa were tested under low constant lateral pressure and axial compression. The cylinders had a diameter of 100 mm and were 200 mm high. The axial stress—axial strain curves of three of the cylinders published by Attard and Setunge are reproduced and predicted using the proposed confined concrete models. The confinement ratios for the cylinder results ranged from 0.04 to 0.14, which place them in the LH range. The three cylinders were of unconfined concrete strength of 110 MPa, subjected to confining pressures of 5, 10, and 15 MPa, respectively. The predictions of the confinement models agree well with the experimental data, as can be seen in Fig. 3 and Table 6.

#### Imran and Pantazopoulou (1996)

The cylinders tested were 55 mm in diameter and 110 mm high, and the concrete strength of the cylinders shown here at the time of testing was 73.4 (“dry” cylinders). Seven of those cylinders were tested at constant lateral pressure and axial compression (type a testing, as described in their paper). The lateral pressure ratios were 0, 3.2, 6.4, 12.8, 25.6, 38.4, and 51.2 MPa. The specimens were classified into the LH and HH categories. The stress-

Table 6. Experimental and Analytical Curve Parameters of Attard-Setunge Curves

$f_c'$ (MPa)	$f_{cl}$ (MPa)	Analytical								Experimental			
		$\epsilon_{co}$ (10-3)	$\epsilon_{cc}$ (10-3)	$\epsilon_{c80}$ (10-3)	$k_d$ (10+8)	$f_{cc}$ (MPa)	$\epsilon_{co}$ (10-3)	$\epsilon_{cc}$ (10-3)	$\epsilon_{c80}$ (10-3)	$f_{cc}$ (MPa)	$\frac{f_{cc}(\text{analytical})}{f_{cc}(\text{experimental})}$	$\frac{\epsilon_{cc}(\text{analytical})}{\epsilon_{cc}(\text{experimental})}$	
110	5	2.43	3.72	6.24	7.77	140.5	2.90	3.80	5.20	150.0	0.94	0.98	
—	10	2.43	5.01	8.84	4.66	165.2	2.90	4.70	7.20	171.3	0.96	1.07	
—	15	2.43	6.30	11.43	3.32	186.9	2.90	5.35	9.80	192.0	0.97	1.18	

**Table 7.** Experimental and Analytical Curve Parameters of Imran-Pantazopoulou Curves

Analytical						Experimental							
$f'_c$ (MPa)	$f_{cl}$ (MPa)	$\epsilon_{co}^a$ (10-3)	$\epsilon_{cc}$ (10-3)	$\epsilon_{c80}$ (10-3)	$k_d$ (10+8)	$f_{cc}$ (MPa)	$\epsilon_{cl}^b$ (10-3)	$\epsilon_{co}$ (10-3)	$\epsilon_{cc}$ (10-3)	$f_{cc}$ (MPa)	$\epsilon_{cl}^b$ (10-3)	$\frac{f_{cc}(\text{analytical})}{f_{cc}(\text{experimental})}$	$\frac{\epsilon_{cc}(\text{analytical})}{\epsilon_{cc}(\text{experimental})}$
73.4	0.00	3.43	3.43	5.15	4.58	73.4	-2.37	3.25	3.25	73.4	-1.54	1.00	1.06
—	3.20	3.43	5.81	11.94	0.54	90.0	-3.71	3.25	4.95	96.1	-3.05	0.94	1.17
—	6.40	3.43	8.19	18.74	0.24	103.9	-5.05	3.25	6.50	108.7	-3.78	0.96	1.26
—	12.80	3.43	12.96	32.34	0.11	127.9	-7.77	3.25	10.45	125.6	-5.28	1.02	1.24
—	25.60	3.43	22.48	59.53	0.05	173.1	-13.57	3.25	20.25	168.6	-8.62	1.03	1.11
—	38.40	3.43	32.01	86.72	0.04	209.0	-19.20	3.25	31.05	204.0	-8.84	1.02	1.03
—	51.20	3.43	41.53	113.91	0.03	241.7	-26.03	3.25	40.90	240.5	-29.33	1.01	1.02

<sup>a</sup>Calculated using  $\epsilon_{co} = 2f'_c / E_c$ .

<sup>b</sup>Lateral strain at peak stress.

strain responses are shown in Fig. 4 and Table 7. It was found that the prepeak axial stress–axial strain response was less stiff than the experimental response, but the lateral deformation trend was well captured by the dilatation model, as expected.

**Karabinis and Rousakis (2002)**

The testing program carried out consisted of concrete cylinders of 200 mm diameter and 320 mm high, wrapped with CFRP (fabric). The cylinders were wrapped with 1, 2, and 3 layers of fiber, whose properties are given in Table 8. The wraps were oriented perpendicular to the longitudinal axis of the cylinder in such a way that they did not contribute to the axial resistance of the confined specimen, and only lateral confinement was provided. The concrete properties of these series are also shown in Table 8.

The cylinders were subjected to axial compression,  $\epsilon_{ju}$  is the rupture strain of the CFRP, and the thickness is given per layer. Three of the tested cylinders were selected for modeling using the in-house nonlinear finite-element program VecTor6 developed for this work. Analyses of these tests serve two purposes: to establish the capacity of the material models to reproduce the incremental lateral pressure due to the confining fabric, and to check the features of the program VecTor6. The analytical model is shown in the inset in Fig. 5; one-quarter of the cylinder was used to reproduce the behavior due to symmetry, and imposed displacements were applied at the top of the cylinder.

The experimental values for the material properties of concrete and CFRP were utilized in the model. The mesh has 160 four-node tori, and the CFRP layers were modeled using “ring” bars attached to the lateral surface nodes of the tori (perfect bond assumed). The area of the ring bar was equivalent to the tributary

area between nodes of the CFRP supplied. The experimental and analytical axial stress–axial strain curves for Type A cylinders (C1, C7, and C13) are shown in Fig. 5. Table 9 compares the experimental results published by Karabinis and Rousakis and those obtained with the program VecTor6. Note that none of these experimental results were used in the formulation of the models, and therefore the results represent a realistic confirmation of the capabilities of the models to reproduce FRP confinement at the material level.

**Conclusion**

A new set of constitutive material models for concrete in confined compression is proposed; the models include formulations to predict the concrete strength enhancement due to triaxial compressive stresses, the peak strain, concrete dilatation, a pre- and postpeak stress-strain curve, and a modified Ottosen failure surface that now takes into account a wide range of concrete strengths and confinement levels. Four simple categories of confined concrete were defined based on the confinement ratio and the concrete type, and the models were used to reproduce the lateral and axial strain–axial stress curves of concrete cylinders tested by different researchers, subjected to axial compression and active lateral pressure. Three cylinders wrapped with FRP fabric and tested in axial compression were also modeled using an in-house program developed for this work; the analytical response of these cylinders showed the capacity of the models and the non-

**Table 8.** Material Properties of Karabinis and Rousakis Cylinders

		Type A
CFRP		
Weight (g/m <sup>2</sup> )	200	—
Thickness (mm)	0.117	—
$E_j$ (MPa)	240,000	—
$\epsilon_{ju}$ (10-3)	0.0155	—
Concrete		
$f'_c$ (MPa)	—	38.5
$E_c$ (MPa)	—	24,500
$\epsilon_{co}$ (10-3)	—	0.00280

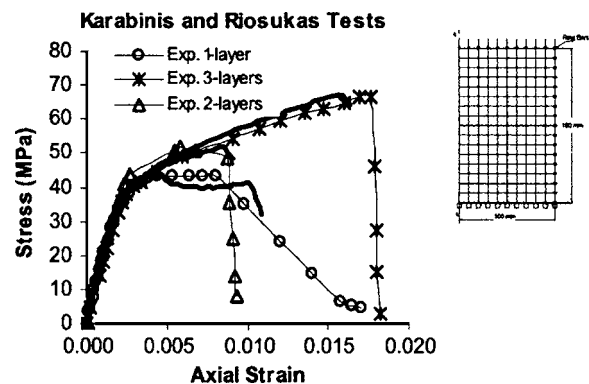


**Fig. 5.** Experimental and analytical stress-strain curves (Type A) and finite-element mesh, Karabinis and Rousakis tests

**Table 9.** Comparison of Experimental and Analytical Results, Karabinis and Rousakis Tests

Cylinder Type A		Strength		Strength gain (%)	Ultimate strain $\epsilon_{cu}$	$\epsilon_{cu}/\epsilon_{co}$	
		(MPa)	Analytical/experimental			Analytical/experimental	
C1 (1 layer)	Experimental	43.0	1.01	12.0	7.96	2.84	1.28
	Analytical	43.6		13.6	10.20	3.64	—
C7 (2 layers)	Experimental	51.5	1.01	34.0	8.77	3.13	0.97
	Analytical	52.0		35.3	8.50	3.04	—
C13 (3 layers)	Experimental	67.0	1.00	74.0	17.60	6.29	0.90
	Analytical	67.2		74.5	15.90	5.68	—

linear finite-element program to reproduce the confined behavior of concrete at the material level. The set of constitutive models follows a compression field approach suitable for implementation in nonlinear finite-element analysis programs based on nonlinear elasticity and damage mechanics.

### Acknowledgments

The first writer is grateful for the financial assistance provided by the National Science and Engineering Research Council of Canada (NSERC) and the University of Toronto and the Government of Ontario, Canada, through an OGSST scholarship.

### References

- Ansari, F., and Li, Q. (1998). "High-strength concrete subjected to triaxial compression." *ACI Mater. J.*, 95(6), 747–755.
- Assa, B., Nishiyama, M., and Watanabe, F. (2001a). "New approach for modeling confined concrete. I: Circular columns." *J. Struct. Eng.*, 127(7), 743–750.
- Assa, B., Nishiyama, M., and Watanabe, F. (2001b). "New approach for modeling confined concrete. II: Rectangular columns." *J. Struct. Eng.*, 127(7), 751–757.
- Attard, M. M., and Setunge, S. (1996). "Stress-strain relationship of confined and unconfined concrete." *ACI Mater. J.*, 93(5), 432–442.
- Candappa, D. C., Sanjayan, J. G., and Setunge, S. (2001). "Complete triaxial stress-strain curves of high-strength concrete." *Coll. Math. J.*, 13(3), 209–215.
- Candappa, D. P., Setunge, S., and Sanjayan, J. G. (1999). "Stress versus strain relationship of high-strength concrete under high lateral confinement." *Cem. Concr. Res.*, 29, 1977–1982.
- Chen, W. F. (1982). *Plasticity in reinforced concrete*, 1st Ed., McGraw-Hill, New York.
- Demers, M., and Neale, K. W. (1999). "Confinement of reinforced concrete columns with fibre-reinforced composite sheets—An experimental study." *Can. J. Civ. Eng.*, 26, 226–241.
- Gardner, N. J. (1969). "Triaxial behavior of concrete." *ACI J.*, 66(15), 136–146.
- Ghazi, M., Attard, M. M., and Foster, S. J. (2002). "Modeling triaxial compression using the microplane formulation for low confinement." *Compos. Struct.*, 80, 919–934.
- Hoshikuma, J., Kazuhiko, K., Kazuhiko, N., and Taylor, A. W. (1996). "A model for confinement effect on stress-strain relation of reinforced concrete columns for seismic design." *Proc., 11th World Conf. on Earthquake Engineering*, Elsevier Science, London.
- Imran, I., and Pantazopoulou, S. J. (1996). "Experimental study of plain concrete under triaxial stress." *ACI Mater. J.*, 93(6), 589–601.
- Karabinis, A. I., and Rousakis, T. C. (2002). "Concrete confined by FRP material: A plasticity approach." *Eng. Struct.*, 24, 923–932.
- Kupfer, H., Hilsdorf, H. K., and Rusch, H. (1969). "Behavior of concrete under biaxial stresses." *ACI J.*, 66(52), 656–666.
- Lee, Y.-H., Willam, K., and Kang, H.-D. (1997). "Experimental observations of concrete behavior under uniaxial compression." Civil and Architectural Engineering Dept., Univ. of Colorado, Boulder, Colo.
- Mander, J. B., Priestley, M. J. N., and Park, R. (1988). "Observed stress-strain behavior of confined concrete." *J. Struct. Eng.*, 114(8), 1827–1849.
- Montgomery, D. L. (1996). "Behavior of spirally reinforced high-strength concrete columns." MSc thesis, Univ. of Toronto, Toronto.
- Montoya, E. (2003). "Behavior and analysis of confined concrete." Ph.D. thesis, Univ. of Toronto, Toronto.
- Montoya, E., Vecchio, F. J., and Sheikh, S. A. (2001). "Compression field modeling of confined concrete." *Struct. Eng. Mech.*, 12(3), 231–248.
- Pessiki, S., Graybeal, B., and Mudlock, M. (2001). "Proposed design of high-strength spiral reinforcement in compression members." *ACI Struct. J.*, 98(6), 799–810.
- Pivonka, P., Lackner, R., and Mang, H. (2000). "Numerical analyses of concrete subjected to triaxial compressive loading." *European Congress on Comp. Methods in Applied Mech.*, ECCOMAS 2000, Barcelona, 26.
- Razvi, S., and Saatcioglu, M. (1999). "Confinement model for high-strength concrete." *J. Struct. Eng.*, 125(3), 281–289.
- Richart, F. E., Brandtzaeg, A., and Brown, R. L. (1928). "A study of the failure of concrete under combined compressive stresses." *Univ. of Illinois Bulletin*, 185.
- Sankarasubramanian, G., and Rajasekaran, S. (1996). "Constitutive modeling of concrete using a new failure criterion." *Compos. Struct.*, 58(5), 1003–1014.
- Sfer, D., Carol, I., Gettu, R., and Etse, G. (2002). "Study of the behavior of concrete under triaxial compression." *J. Eng. Mech.*, 128(2), 156–163.
- Sheikh, S. A., and Uzumeri, S. M. (1980). "Strength and ductility of tied concrete columns." *ASCE J. Struct. Div.*, 106(5), 1079–1102.
- Toklucu, M. T. (1992). "Behavior of reinforced concrete columns confined with circular spiral and hoops." MSc thesis, Univ. of Toronto, Toronto.
- Tume, J. (1987). *Engineering mathematics handbook*, 3rd Ed., McGraw-Hill, New York.
- Xie, J., Elwi, A. E., and MacGregor, J. G. (1995). "Mechanical properties of three high-strength concretes containing silica fume." *ACI Mater. J.*, 92(2), 135–145.